INL/CON-15-36442
PREPRINT

Hybrid P_N-S_N Calculations with SAAF for the Multiscale Transport Capability in Rattlesnake

PHYSOR 2016

Yaqi Wang, Sebastian Schunert,
Mark DeHart, Richard Martineau

May 2016

The INL is a
U.S. Department of Energy
National Laboratory
operated by
Battelle Energy Alliance

Hybrid P_N-S_N Calculations with SAAF for the Multiscale Transport Capability in Rattlesnake.

Yaqi Wang[1]*, Sebastian Schunert[1], Mark DeHart[2], Richard Martineau[3]
[1]Thermal Science & Safety Analysis, Idaho National Laboratory, Idaho Falls, ID, USA
[2]Reactor Physics Analysis & Design, Idaho National Laboratory, Idaho Falls, ID, USA
[3]Modeling & Simulation, Idaho National Laboratory, Idaho Falls, ID, USA

ABSTRACT

An interface condition for hybrid P_N-S_N calculations is proposed for the self-adjoint angular flux (SAAF) formulation of the transport equation using the continuous finite element method (FEM) for spatial discretization. This interface condition is implemented in Rattlesnake, the radiation transport application built on MOOSE, for the on-going multiscale transport simulation effort at INL. The interface condition uses the mortar FEM framework in MOOSE for spatial coupling that is based on a Lagrange multiplier approach for constraining the solution in angle. For smoothing the solution at the interface a method based on S_N Lagrange interpolation on the sphere is proposed. Numerical results indicate that the interface condition gives the expected convergence.

Key Words: **Hybrid P_N-S_N, Multiscale transport, SAAF, Mortar FEM, Lagrange multiplier**

1. INTRODUCTION

Transport calculations for simulating the neutron behavior in a nuclear reactor core with fine resolution in the seven-dimensional phase space (1 in time, 3 in space, 2 in angle and 1 in energy) will remain a challenge for the foreseeable future. However, fine resolution over the entire core is rarely required or necessary. Typically we can apply higher resolutions in regions of interest, for instance the experiment bundle of TREAT (transient reactor test facility) at INL, and lower resolutions with various homogenization levels everywhere else. Although the solution accuracy of the regions of interest can be bounded by the accuracy of the lower-resolution regions especially close to the interface, it is argued that the accuracy can be significantly improved by taking into account the environmental condition imposed by lower-resolution regions. On the other hand, we can avoid the pre-homogenization of high-resolution regions, which often couldn't be conducted accurately. We will label this approach as the *multiscale* transport methods. Discrete ordinates methods (S_N) are suitable for handling heterogeneous problems due to the decoupling of angular variables in the streaming operators, while the spherical harmonics expansion methods (P_N) typically generate more accurate results with the same

*Corresponding author: yaqi.wang@inl.gov

number of unknowns for problems with significant homogenization. It is believed that regions of different levels of homogenization can be treated most efficiently with the hybrid S_N-P_N calculations. Hybrid S_N-P_N calculations have been studied in the past [1–6]. Among them Ref. [1, 2, 5, 6] are for the one-dimensional. Ref. [3, 4] handles the coupling between VNM (variational nodal method) with P_N and SNM (S_N nodal method), both of which are locally conservative.

Rattlesnake is the radiation transport application built with MOOSE for modern multiphysics simulations. Multiple discretization schemes have been developed in Rattlesnake. Among them, SAAF-CFEM-SN and SAAF-CFEM-PN [7–10] are based on the self-adjoint angular flux formulation (SAAF) with the continuous finite element method (FEM). They differ from each other only by the angular treatment, either S_N or P_N. Similarly we have implemented LS(least square)-CFEM-SN and LS-CFEM-PN [11] for a better void treatment. We also have a first-order S_N method discretized with discontinuous FEM [12, 13], but the deployed transport sweeper requires further optimization. Diffusion approximation with continuous and discontinuous FEM are also available. All of these are developed on top of the general mesh framework with MOOSE supporting multidimensional unstructured mesh with massive parallelization. We want to implement the multiscale transport capability to leverage these transport schemes.

Implementing the multiscale transport capability in a production code is a non-trivial task. It involves three parties: the framework developers, application developers and reactor analysts. In our case, they are the MOOSE developers, Rattlesnake developers and INL Rattlesnake users for the initial deployment, respectively. Although the interface condition for coupling S_N and P_N is special, it contains the common spatial-coupling piece, which can be useful to other physics. For example, mortar FEM for coupling two regions or subdomains has been investigated intensively outside of the transport community [14–17]. Multiscale transport should be able to benefit from the solver development on the framework side as well. The role of application developers is to develop and implement the interface condition and to provide for any special needs, if there are any, to the framework developers. It is also the application developers who are responsible for assuring the good usability by incorporating the feedback from the analysts. Reactor analysts are the end users who create the models for the real reactor simulations: the mesh, cross section library and etc. This paper focuses on the S_N-P_N interface condition, particularly, the coupling between SAAF-SN-CFEM and SAAF-PN-CFEM in the viewpoint of the application developers.

It should be mentioned that the adaptive domain partitioning based on *a posterior* estimation technique as Ref. [5] is not our current interest. Instead, the domain is partitioned by the user before the calculation and the discretization schemes applied on each subdomain is set by the user. Spatial interface conditions are implemented via the general mortar FEM framework available in MOOSE. Leveraging the flexibility of the mortar FEM capability, the meshes on different subdomains can be conforming at the mortar interface but they are not required. A custom MOOSE mesh modifier is used to split conforming meshes behind the scenes and interface conditions are added automatically during the simulation. The only difference in users' perspective is that a separate transport method has to be specified for each subdomain. We will not report CPU times in this study because more efficient solving techniques handling the resultant saddle point problem from the multiscale are under development.

We are exclusively considering the multigroup approximation in energy variable. Embedded energy structures are assumed across two neighboring scales, i.e. any group in these two scales is either a subset or completely outside of another group. Although we will only show the method with one-group steady-state source problem, it can be extended to multigroup transient or eigenvalue problems without any fundamental difficulty. Although users are allowed to amend the interface conditions with the properties defined on interfaces, such as discontinuity factors from the generalized homogenization theory [18], this paper will only talk about the nominal conditions.

The rest of this paper is arranged as follows: Section 2 gives the theory of the condition and Section 3 shows some representing results. Conclusions will be drawn and future works will be discussed at the end.

2. THEORY

We use the following one-group steady-state transport equation with isotropic scattering and external sources to demonstrate our methodology:

$$\vec{\Omega}\cdot\vec{\nabla}\Psi+\sigma_t(\vec{r})\Psi(\vec{r},\vec{\Omega})=\frac{1}{4\pi}\left(\sigma_s(\vec{r})\Phi(\vec{r})+Q(\vec{r})\right),\vec{r}\in\mathcal{D},\vec{\Omega}\in\mathcal{S}, \tag{1}$$

where $\vec{r}$ and $\vec{\Omega}$ are the spatial and angular independent variables defined in the domain $\mathcal{D}$ and on the two-dimensional unit sphere $\mathcal{S}$. Ψ is the angular flux and Φ is the scalar flux defined as $\int_{\mathcal{S}}\Psi d\Omega$. σ_t and σ_s are the total and scattering cross sections respectively. Q is the external source. This equation is solved along with the surface source boundary condition

$$\Psi(\vec{r}_b,\vec{\Omega})=\Psi^{inc}(\vec{r}_b,\vec{\Omega}),\vec{r}_b\in\partial\mathcal{D}_s,\vec{\Omega}\cdot\vec{n}(\vec{r}_b)<0 \tag{2}$$

and/or the reflecting boundary condition

$$\Psi(\vec{r}_b,\vec{\Omega})=\Psi(\vec{r}_b,\vec{\Omega}_r),\vec{r}_b\in\partial\mathcal{D}_r,\vec{\Omega}\cdot\vec{n}(\vec{r}_b)<0, \tag{3}$$

where $\vec{\Omega}_r=\vec{\Omega}-2(\vec{\Omega}\cdot\vec{n})\vec{n}$. There is nothing significant to extend the method to anisotropic scattering and external sources.

We will first state the weak form of the SAAF equations with domain decomposition which takes the form of a convection-reaction equation along a particular angular direction given the directional source. A Lagrange multiplier is introduced for coupling subdomains and its physical meaning is explained. We then move to the full transport weak form including all interface terms. To this end, we define the angular space for the Lagrange multipliers on the interface and derive the interface condition. It has been observed numerically that Lagrange interpolation of S_N solution needs to be constructed to ensure a smooth coupling of S_N and P_N. This smoothing treatment is detailed at the end of this section.

2.1. SAAF Weak Form for the Convection-Reaction Equation with Domain Decomposition

The simple convection-reaction equation defined over a solution domain $\mathcal{D}$ is

$$\vec{\Omega} \cdot \vec{\nabla}\psi + \sigma_t(\vec{r})\psi(\vec{r}) = q(\vec{r}). \tag{4}$$

We use lower case of Ψ and Q for this directional equation. The weak form with SAAF is to find $\psi \in W_{\mathcal{D}}$, such that

$$b_{\vec{\Omega}}(\psi, \psi^*) = l(\psi^*), \qquad \forall \psi^* \in W_{\mathcal{D}}, \tag{5}$$

where

$$b_{\vec{\Omega}}(\psi, \psi^*) \equiv (\frac{1}{\sigma_t}\vec{\Omega} \cdot \vec{\nabla}\psi, \vec{\Omega} \cdot \vec{\nabla}\psi^*)_{\mathcal{D}} + (\psi, \sigma_t\psi^*)_{\mathcal{D}} + \langle \psi, \psi^* \rangle^+ , \tag{6}$$

$$l(\psi^*) \equiv (S, \psi^* + \frac{1}{\sigma_t}\vec{\Omega} \cdot \vec{\nabla}\psi^*)_{\mathcal{D}} + \left\langle \psi^{inc}, \psi^* \right\rangle^- . \tag{7}$$

$W_{\mathcal{D}}$ is a continuous function space in which the solution is sought although the solution may present discontinuity perpendicular to the characteristic lines. Notations used in Eq. (6) and Eq. (7) are defined as,

$$(f, g)_{\mathcal{D}} \equiv \int_{\mathcal{D}} f(\vec{r})g(\vec{r})d\vec{r}, \tag{8}$$

$$\langle f, g \rangle^{\pm} \equiv \int_{\partial\mathcal{D}^{\pm}} \left|\vec{\Omega} \cdot \vec{n}\right| f(\vec{r})g(\vec{r})ds, \tag{9}$$

where $\partial\mathcal{D}^+$ and $\partial\mathcal{D}^-$ are the downwind ($\vec{\Omega} \cdot \vec{n} > 0$) and upwind ($\vec{\Omega} \cdot \vec{n} < 0$) boundary with respect to $\vec{\Omega}$ respectively.

We have an arbitrary domain decomposition $\mathcal{D} = \bigcup_{k=1}^{K} \mathcal{D}_k$ and the interface is given by $\Gamma_{int} = \bigcup_{k=1}^{K}(\bigcup_{j=1}^{K}(\mathcal{D}_k \bigcap \mathcal{D}_j))$. We use a new notation $\bar{W}_D$ for the function space which is now subdomain-wise continuous. We can use the Lagrange multipliers to enforce the continuity:

$$-(\llbracket\psi\rrbracket, \lambda^*)_{\Gamma_{int}} , \tag{10}$$

Without destroying the consistency, we add the term symmetric to the above term

$$-(\llbracket\psi^*\rrbracket, \lambda)_{\Gamma_{int}} , \tag{11}$$

where

$$\psi^{\pm} \equiv \lim_{s\to 0} \psi(\vec{r} \pm s\vec{n}), \tag{12}$$

$$\llbracket\psi\rrbracket \equiv \psi^+ - \psi^-, \tag{13}$$

$$(f, g)_{\Gamma_{int}} \equiv \int_{\Gamma_{int}} f\ g\ ds. \tag{14}$$

$\vec{n}$ is the norm unit vector associated with interior sides and can be arbitrarily oriented.

The bilinear form with the Lagrange multipliers becomes:

$$b_{\vec{\Omega}}(\psi, \lambda, \psi^*, \lambda^*) \equiv b_{\vec{\Omega}}(\psi, \psi^*) - (\llbracket \psi \rrbracket, \lambda^*)_{\Gamma_{int}} - (\llbracket \psi^* \rrbracket, \lambda)_{\Gamma_{int}}, \tag{15}$$

where both λ and λ^* are in a function space denoted with V_Γ. Some further explanations are in order:

1. It can be proved that the above bilinear form yields the same solution ψ as the original one.
2. The physical meaning of the Lagrange multiplier is the angular flux times $\vec{\Omega}\cdot\vec{n}$. However, it could not be equal to $\vec{\Omega}\cdot\vec{n}\psi^{\pm}$ when the analytical solution does not belong to $\bar{W}_{\mathcal{D}}$. Exact subdomain-wise balance is obtained with λ but not with ψ, which can be seen with the subdomain-wise constant test functions.
3. Although with domain decomposition, we do not have to enforce the continuity on the domain interface when $\vec{\Omega}\cdot\vec{n} = 0$. We can develop a Lagrange multiplier having the exact angular flux, but we still want to use the currently form in order to preserve the solution of the original weak form.
4. It is noted that there are ways of introducing null spaces in V_Γ. For instance, if we break the function space on each individual subdomain interface, and there is a node shared by more than two interfaces, then we add one redundant constraints for this node. These null spaces do not affect the solution of angular flux though.
5. The basis function spanning the function space V can be sophisticated for a general mortar FEM. If we have conforming meshes on subdomains, i.e. no hanging nodes on interfaces, we can simply use the non-zero traces of the basis functions of the original space $W_{\mathcal{D}}$.
6. The matrix structure resulted from the above weak form is a typical saddle point matrix:

$$\begin{bmatrix} \mathbf{A} & \mathbf{B}^T \\ \mathbf{B} & 0 \end{bmatrix} \begin{bmatrix} \boldsymbol{\psi} \\ \boldsymbol{\lambda} \end{bmatrix} = \begin{bmatrix} \mathbf{b} \\ 0 \end{bmatrix},$$

   where the normal streaming, collision and boundary terms are assembling the invertible block diagonal matrix $\mathbf{A}$, where each block is corresponding to a subdomain.

2.2. SAAF PN-SN Weak Form and the Interface Condition

After the integration of simple transport equations, Eqs. (6) and (7), of all directions, we obtain

$$b(\Psi, \Psi^*) = l(\Psi^*) \tag{16}$$

where

$$b(\Psi,\Psi^*)\equiv\int_{\mathcal{S}}\left[\left(\vec{\Omega}\cdot\vec{\nabla}\Psi^*,\frac{1}{\sigma_t}\vec{\Omega}\cdot\vec{\nabla}\Psi\right)_{\mathcal{D}}+(\Psi^*,\sigma_t\Psi)_{\mathcal{D}}\right]d\Omega-\int_{\mathcal{S}}d\Omega\left(\Psi^*+\frac{1}{\sigma_t}\vec{\Omega}\cdot\vec{\nabla}\Psi^*,\frac{\Phi}{4\pi}\right)_{\mathcal{D}}+\int_{\vec{\Omega}\cdot\vec{n}>0}d\Omega\left\langle\Psi^*,\Psi\right\rangle_{\partial\mathcal{D}}-\int_{\vec{\Omega}\cdot\vec{n}<0}d\Omega\left\langle\Psi^*,\Psi(\vec{\Omega}_r)\right\rangle_{\partial\mathcal{D}_r},\tag{17}$$

$$l(\Psi^*)\equiv\int_{\vec{\Omega}\cdot\vec{n}<0}d\Omega\left\langle\Psi^*,\Psi^{inc}\right\rangle_{\partial\mathcal{D}_s}+\int_{\mathcal{S}}d\Omega\left(\Psi^*+\frac{1}{\sigma_t}\vec{\Omega}\cdot\vec{\nabla}\Psi^*,Q\right)_{\mathcal{D}}.\tag{18}$$

Ψ belongs to a function space $W_{\mathcal{D}}\otimes S$, where S is the angular space. The weak form with domain decomposition for the SAAF is to find a solution Ψ in a function space $\bar{W}_{\mathcal{D}}\otimes S$ and Λ in $\bar{V}_{\Gamma}\otimes S$, such that $\forall\Psi^*$ and Λ^* in the same corresponding function space

$$b(\Psi,\Lambda,\Psi^*,\Lambda^*)=l(\Psi^*),\tag{19}$$

where

$$b(\Psi,\Lambda,\Psi^*,\Lambda^*)\equiv b(\Psi,\Psi^*)-\int_{\mathcal{S}}\left[(\llbracket\Psi\rrbracket,\Lambda^*)_{\Gamma_{int}}+(\llbracket\Psi^*\rrbracket,\Lambda)_{\Gamma_{int}}\right]d\Omega.\tag{20}$$

We define the two subdomains as

$$\mathcal{D}_{SN}=\{\vec{r}\in\mathcal{D},\text{where SN is applied}\},\tag{21}$$

$$\mathcal{D}_{PN}=\{\vec{r}\in\mathcal{D},\text{where PN is applied}\}.\tag{22}$$

On $\mathcal{D}_{SN}$, we solve the equation in a given set of directions specified by an angular quadrature $\left\{\vec{\Omega}_m,w_m,m=1,\cdots,M\right\}$. We will denote angular flux on $\vec{\Omega}_m$ as $\Psi_m(\vec{r})$ and all the angular fluxes as $\vec{\Psi}$. On $\mathcal{D}_{PN}$, we let S be spanned by the spherical harmonics up to order N. Angular flux in this space can be represented as $\Psi=\vec{\mathbf{R}}^T(\vec{\Omega})\vec{\Phi}(\vec{r})$, where $\vec{\Phi}$ is the column vector of all angular flux moments and $\vec{\mathbf{R}}$ is the spherical harmonics $\vec{\mathbf{Y}}$ times the normalization factors, i.e.

$$\vec{\mathbf{R}}=\mathbf{P}\vec{\mathbf{Y}},\tag{23}$$

where $\mathbf{P}=\left(\int_{\mathcal{S}}\vec{\mathbf{Y}}\vec{\mathbf{Y}}^T d\Omega\right)^{-1}$ is diagonal and composing of all normalization factors. Because typically the dimension of P_N angular space is smaller, we let the S_N side as the master, i.e. we make the unit norm of the interface n always point toward to S_N side. We will skip the detailed weak forms on both $\mathcal{D}_{SN}$ and $\mathcal{D}_{PN}$. The boundary needs to be split with S_N and P_N.

Now, we need to handle the term on S_N-P_N domain interface $\Gamma=\partial\mathcal{D}_{PN}\cap\partial\mathcal{D}_{SN}$:

$$\int_{\mathcal{S}}\left((\llbracket\Psi\rrbracket,\Lambda^*)_{\Gamma}+(\llbracket\Psi^*\rrbracket,\Lambda)_{\Gamma}\right)d\vec{\Omega}.\tag{24}$$

We will use the same angular space of the S_N side for the Lagrange multiplier, i.e. we have $\{\Lambda_m, \Lambda_m^*, m = 1, \cdots, M\}$. On the S_N side,

$$\sum_{m=1}^{M} w_m \left((\Psi_m, \Lambda_m^*)_\Gamma + (\Psi_m^*, \Lambda_m)_\Gamma \right). \tag{25}$$

On the P_N side,

$$-\sum_{m=1}^{M} w_m \left(\vec{\mathbf{R}}^T(\vec{\Omega}_m)\vec{\mathbf{\Phi}}, \Lambda_m^* \right)_\Gamma - \left(\vec{\mathbf{\Phi}}^*, \mathbf{P}\vec{\mathbf{\Lambda}} \right)_\Gamma, \tag{26}$$

where

$$\vec{\mathbf{\Lambda}} \equiv \sum_{m=1}^{M} w_m \vec{\mathbf{Y}}(\vec{\Omega}_m)\Lambda_m. \tag{27}$$

It is noted that if the angular quadrature can integrate spherical harmonics up to order $N_{SN} > N$, the first term in Eq. (25) and Eq. (26) will ensure the continuity of the angular flux moments. It also will cause all the flux moments evaluated on the S_N side with order being greater than N and less equal to N_{SN} to be zero. However, the above interface condition creates non-smooth PN solutions close to the interface based on observations in numerical experiments.

2.3. SN Lagrange Interpolation for the Interface Condition

It is noted that the angular function space on the S_N side is not clearly defined so far. Different interpolation schemes can be applied to construct the space, or to construct the solution over the sphere, with M discrete angular fluxes. One way of achieving this is through Lagrange interpolation. We let the constructed flux in a space spanned by the spherical harmonics with the dimension being the number of directions M. We will denote the set of these basis spherical harmonics as $\vec{\mathbf{Y}}$. It is noted that the spherical harmonics on the P_N side will always be a subspace of the above space. Then we can more or less freely select some spherical harmonics in the $L > N$ space to make the dimension equal to M. If level-symmetric quadrature with S_N is used, Ref. [19] suggested that the following space $\vec{\mathbf{Y}} = \left\{ Y_{l,m}, 0 \le m \le l; 0 \le l \le \bar{N} - 1; m \text{ is odd and } 0 < m < \bar{N} \text{ with } l = \bar{N} \right\}$ for two-dimensional calculations if level-symmetric quadrature is used. Here $\bar{N}$ is the level-symmetric S_N order.

We denote the sphere nodal function associated with direction m as $L_m(\vec{\Omega})$. $L_m(\vec{\Omega})$ satisfies the following conditions

$$L_m(\vec{\Omega}_{m'}) = \delta_{m,m'}, \qquad m' = 1, \cdots, M \tag{28}$$

We expand the nodal functions as

$$L_m(\vec{\Omega}) = \vec{\mathbf{R}}^T(\vec{\Omega})\vec{\mathbf{a}}_m, \tag{29}$$

and form the following linear equation from the conditions,

$$\mathbf{R}\vec{\mathbf{a}}_m = \vec{\mathbf{e}}_m, \tag{30}$$

where $R_{m,m'} = R_{m'}(\vec{\Omega}_m)$. If we define $\mathbf{A} = \{\vec{a}_1, \vec{\mathbf{a}}_2, \cdots, \vec{\mathbf{a}}_M\}$, we have

$$\mathbf{RA} = \mathbf{I}. \tag{31}$$

The constructed angular flux

$$\Psi(\vec{\Omega}) = \sum_{m=1}^{M} \Psi_m L_m(\vec{\Omega}) = \sum_{m=1}^{M} \Psi_m \vec{\mathbf{R}}^T(\vec{\Omega})\vec{\mathbf{a}}_m = \vec{\mathbf{R}}^T(\vec{\Omega})\mathbf{A}\vec{\mathbf{\Psi}} \tag{32}$$

From the constructed angular flux, we can evaluate the angular moments

$$\vec{\mathbf{\Phi}} \equiv \int_{\mathcal{S}} \vec{\mathbf{Y}}(\vec{\Omega})\Psi(\vec{\Omega})d\Omega = \mathbf{A}\vec{\mathbf{\Psi}}. \tag{33}$$

Typically the angular flux moments evaluated using Eq. (33) is different from the one directly evaluated from the angular quadrature. We want to use

$$\vec{\mathbf{\Lambda}} = \sum_{m=1}^{M} \vec{\mathbf{A}}_m \Lambda_m, \tag{34}$$

where $\vec{\mathbf{A}}_m$ is the m-th row of the matrix $\vec{\mathbf{A}}$. We will use Eq. (34) for the interface condition in Eq. (26).

Before closing this section, it is worthwhile to mention that the interface conditions for P_N-P_N with different orders can be implemented by making the Lagrange multiplier angular space the same as the angular space with the higher P_N order. The Lagrange multiplier essentially make all the angular moments of the lower P_N order continuous across the interface and the higher angular moments on the higher P_N order side zero. SAAF-CFEM-P0 is equivalent with the diffusion approximation if the boundary condition is imposed in a way of decoupling the even and odd parities. Both SAAF-CFEM-SN and SAAF-CFEM-PN interface condition with diffusion continuous FEM are tested and working.

3. Numerical Results

We tested the implemented interface condition with a one-group homogeneous fixed-source problem. The domain is $8cm \times 8cm$ discretized by a 8-by-8 uniform Cartesian grid. Total and scattering cross sections are uniform, $1cm^{-1}$ and $0.9cm^{-1}$ respectively, and the external source is isotropic and uniform with $1cm^{-3}s^{-1}$. Left, right and top boundaries are reflecting and the bottom boundary is vacuum. The problem is illustrated in Fig. 1. It should be pointed out that the exact scalar flux is constant along lines with $y = const$. We divide the domain into two subdomains by the line starting through $(0, 6)cm$ and

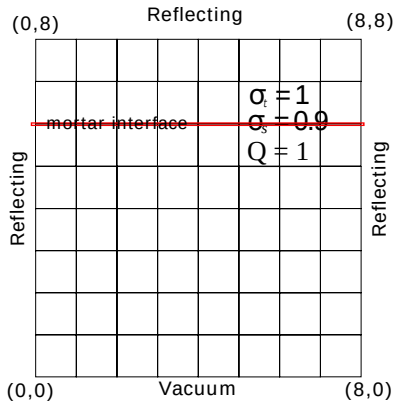

Figure 1: A one-group homogeneous problem.

$(6, 6)cm$ and apply SAAF-CFEM-SN at the lower part and SAAF-CFEM-PN at the upper part. Level-symmetric angular quadratures of orders ranging from 8 to 18 are used for the angular discretization within the SAAF-CFEM-SN subdomain. Within the SAAF-CFEM-PN subdomain, P_N orders ranging from 0 to 6 are used. For the solution of the equation system resulting from the FEM discretization, we exclusively employ the PJFNK (preconditioned Jacobian-free Newton-Krylov) solver in this study. The preconditioning matrix comprises contributions from the streaming, collision, vacuum boundary condition, and the interface terms. We gathered the relative errors of integration of scalar flux in the lower part and upper part with the corresponding S_N solution over the entire domain into Table I and Table II. The last row of these two tables show the the relative error between the S_N solution and the reference solution $379.046cm/s$ and $156.31848cm/s$ generated with S24 all on the entire domain.

Table I: Relative error of the lower integrated scalar flux.

P_N order	S_N order 8	10	12	14	16	18
0	1.93E-04	1.93E-04	1.93E-04	1.93E-04	1.93E-04	1.93E-04
1	2.07E-04	2.07E-04	2.07E-04	2.07E-04	2.07E-04	2.07E-04
2	3.68E-06	3.62E-06	3.60E-06	3.59E-06	3.58E-06	3.58E-06
3	-1.71E-06	-1.77E-06	-1.80E-06	-1.81E-06	-1.81E-06	-1.82E-06
4	4.59E-09	1.67E-08	1.78E-08	1.68E-08	1.76E-08	1.74E-08
5	7.82E-09	1.82E-08	1.97E-08	1.86E-08	2.00E-08	1.98E-08
6	-5.63E-09	1.55E-09	8.04E-10	-1.09E-09	-2.22E-10	-8.34E-10
	-8.68E-04	-5.78E-04	-3.83E-04	-2.70E-04	-1.80E-04	-1.21E-04

We can see that the integrated flux at the lower part has larger angular discretization error than the one at the upper part because of the stronger transport effect close to the vacuum boundary. With a fixed S_N order, errors drop with the increased P_N order. For all S_N orders, the errors with different P_N orders are very close except the P_N order 6 or P_N order larger than 4 with S8, possibly due to the contamination with the iterative error. We see significant error drop for N to $N + 1$ when N is odd,

Table II: Relative error of the upper integrated scalar flux.

P_N order	S_N order 8	10	12	14	16	18
0	-5.30E-04	-5.31E-04	-5.31E-04	-5.31E-04	-5.31E-04	-5.31E-04
1	-5.80E-04	-5.81E-04	-5.81E-04	-5.81E-04	-5.81E-04	-5.81E-04
2	-1.01E-05	-1.00E-05	-9.95E-06	-9.93E-06	-9.93E-06	-9.93E-06
3	3.57E-06	3.72E-06	3.79E-06	3.81E-06	3.82E-06	3.82E-06
4	-2.88E-08	-5.93E-08	-6.15E-08	-5.89E-08	-6.11E-08	-6.04E-08
5	-2.10E-08	-4.67E-08	-4.93E-08	-4.64E-08	-4.99E-08	-4.92E-08
6	1.35E-08	-4.84E-09	-1.79E-09	3.28E-09	1.09E-09	2.88E-09
	-4.55E-05	-3.07E-05	-2.05E-05	-1.46E-05	-9.77E-06	-6.57E-06

which can be explained by the weak coupling from odd parity to even parity at the boundaries [10].

The flux of S16-P4 are plotted in Fig. 2a along with its contour lines. We can see the scalar flux are continuous across the mortar interface and the solution is relatively flat along the x direction even though it is not exactly constant. The same solution but with the interface condition in Eq. (26) are plotted in Fig. 2b. We can clearly see the non-smoothness of the solution along the interface. The solution is indeed symmetric with respect to the line at $(4, 0)cm$ to $(4, 8)cm$, which is not the case indicated by the color rendering during visualization.

We then rotated the mesh with $45°$ to test if the rotation can severely impact the validity of the implemented interface condition. $45°$ makes all the reflecting directions on the left, right and top boundaries are still in the quadrature. The solution is indeed affected by the rotation, for example, the integrated fluxes at the lower part and upper part are $379.245510cm/s$ and $156.323143cm/s$ from those un-rotated $378.977864cm/s$ and $156.316943cm/s$. The flux are plotted in Fig. 2c. Color bars show the the same limits of the fluxes as in Fig. 2a. We can see that the interface condition is still working properly, i.e., the solution remains continuous across and smooth along the mortar interface.

4. CONCLUSION

We presented the interface condition for hybrid S_N and P_N calculations with SAAF and continuous FEM. Particle conservation with the Lagrange multiplier defined on the subdomain interfaces is achieved subdomain-wise. Lagrange interpolation on sphere are proposed to smooth the transition of the S_N and P_N solutions on the interfaces. A one-group homogeneous steady-state source problem shows the interface condition works properly and does not depend on the mesh rotation. We would like to test the hybrid calculations with more sample problems, either multigroup eigenvalue or transient, with or without group collapsing in the future. We will also show the CPU-time results with the fine-tuned mortar FEM framework and solvers of the saddle point problems. Ultimately, we will

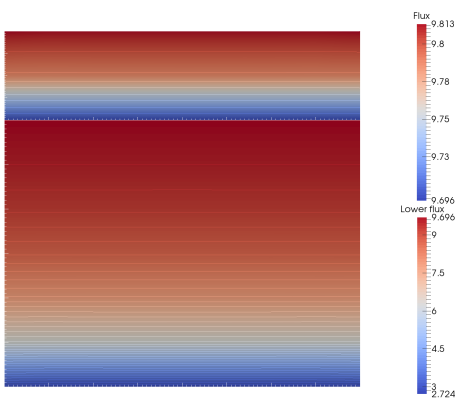

(a) With Eq. (34).

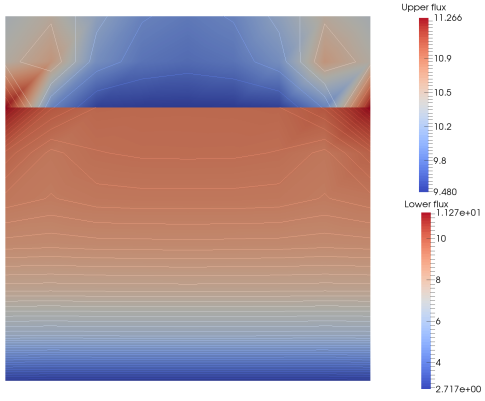

(b) With Eq. (26).

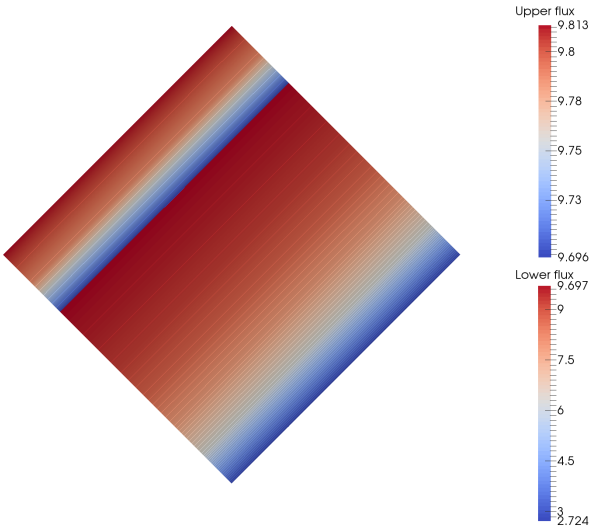

(c) With 45 degree rotation of the mesh.

Figure 2: Flux with S16 and P4.

apply the multiscale transport capability in Rattlesnake for applications to the real reactors like ATR (advanced test reactor) and TREAT at INL.

ACKNOWLEDGMENTS

This work is supported by the U.S. Department of Energy, under DOE Idaho Operations Office Contract DE-AC07-05ID14517. Accordingly, the U.S. Government retains a nonexclusive, royalty-free license to publish or reproduce the published form of this contribution, or allow others to do so, for

U.S. Government purposes. The authors also thank David Andrs, one of the MOOSE developers, Dmitry Karpeyev at ANL for the mortar FEM works they have done in MOOSE. The authors also thank Javier Ortensi, Frederick N. Gleicher and Gilles J Youinou at INL for their fruitful discussions on the application of the multiscale transport.

REFERENCES

[1] M. M. Nanneh and M. M. R. Williams. "A diffusion-transport theory hybrid method for calculating neutron flux distributions in slab lattices." *Atomkernenergie Kerntechnik*, **47**: pp. 221–224 (1985).

[2] R. C. Barros *et al.* "Progress in spectral nodal methods applied to discrete ordinates transport problems." *Progress in Nuclear Energy*, **33(1/2)**: pp. 117–154 (1998).

[3] E. Girardi and J.-M. Ruggieri. "Mixed first- and second-order transport method using domain decomposition techniques for reactor core calculations." In: *Proc. International Conference on Supercomputing in Nuclear Application*. Paris, France (2003).

[4] E. Girardi *et al.* "A new method for the treatment of local strong heterogeneities and its application to the phebus experimental facility." In: *PHYSOR 2004 - The Physics of Fuel Cycles and Advanced Nuclear Systems : Global Developments*. American Nuclear Society, Lagrange Park, IL, Chicago, Illinois (2004).

[5] D. Y. Anistratov and N. D. Stehle. "Computational transport methodology based on decomposition of a problem domain into transport and diffusive subdomains." *Journal of Computational Physics*, **231**: pp. 8009–8028 (2012).

[6] S. Manolov, J. E. Morel, and C. Rabiti. "Hybrid Sn-diffusion and Sn-P3 transport calculations." In: *International Conference on Mathematics and Computational Methods Applied to Nuclear Science and Engineering*, (pp. 2748–2758). Sun Valley, Idaho (2013).

[7] Y. Wang, H. Zhang, and R. Martineau. "Diffusion acceleration schemes for the self-adjoint angular flux formulation with a void treatment." *Nuclear Science and Engineering*, **176**: pp. 201–225 (2014).

[8] Y. Wang. "Nonlinear diffusion acceleration for the multigroup transport equation discretized with s_n and continuous FEM with Rattlesnake." In: *International Conference on Mathematics and Computational Methods Applied to Nuclear Science and Engineering*, (pp. 2648–2665). Sun Valley, Idaho (2013).

[9] S. Schunert *et al.* "A new mathematical adjoint for the modified saaf-sn equations." *Annals of Nuclear Energy*, **75**: pp. 340–352 (2015).

[10] Y. Wang and F. N. Gleicher. "Revisit boundary conditions for the self-adjoint angular flux formulation." In: *PHYSOR 2014 - The Role of Reactor Physics toward a Sustainable Future*. The Westin Miyako, Kyoto, Japan (2014).

[11] J. Hansen *et al.* "A least-squares transport equation compatible with voids." *Journal of Computational and Theoretical Transport Special Issue: Papers from the 23rd International Conference on Transport Theory*, **43(1–7)** (2014).

[12] S. Schunert *et al.* "A high-order nonlinear diffusion acceleration for the SN equations discretized with the discontinuous FEM I: Theory and numerical results." *Transactions of the American Nuclear Society*, **113(1)**: pp. 677–679 (2015).

[13] —. "A high-order nonlinear diffsion acceleration for the SN equations discretized with the discontinuous FEM II: Fourier analysis." *Transactions of the American Nuclear Society*, **113(1)**: pp. 680–683 (2015).

[14] F. B. Belgacem. "The mortar finite element method with lagrange multipliers." *Numerische Mathematik*, **84**: pp. 173–197 (1999).

[15] D. Braess, W. Dahmen, and C. Wieners. "A multigrid algorithm for the mortar finite element method." *SIAM Journal on Numerical Analysis*, **37(1)**: pp. 48–69 (1999).

[16] B. I. Wohlmuth. "A mortar finite element method using dual spaces for the lagrange multiplier." *SIAM Journal on Numerical Analysis*, **38(3)**: pp. 989–1012 (2000).

[17] C. Kim *et al.* "Multiplier spaces for the mortar finite element method in three dimensions." *SIAM Journal on Numerical Analysis*, **39(2)**: pp. 519–538 (2001).

[18] K. S. Smith. "Assembly homogenization techniques for light water reactor analysis." *Progress in Nuclear Energy*, **17,3**: pp. 303–335 (1986).

[19] W. F. Miller, Jr. and W. H. Reed. "Ray-effect mitigation methods for two-dimensional neutron transport theory." *Nuclear Science and Engineering*, **62**: pp. 391–411 (1977).